ELSEVIER

Journal of Nuclear Materials 312 (2003) 212–223

journal of nuclear materials

www.elsevier.com/locate/jnucmat

Mechanical properties and microstructure of helium-implanted beryllium

W. Kesternich *, H. Ullmaier

Institut für Festkörperforschung, Forschungszentrum Jülich, 52425 Jülich, Germany

Received 4 June 2002; accepted 21 November 2002

Abstract

0.2 mm thick specimens of beryllium have been homogeneously implanted with helium. Implantation temperatures ranged from 100 to 600 °C, and final helium concentrations from 30 to 800 appm. Tensile tests at temperatures between 20 and 600 °C were carried out with testing temperature both equal to and lower than the implantation temperatures. For practicality all conditions of helium-implanted specimens, ductility decreased and yield and ultimate tensile strength increased as compared to the unimplanted specimens. The amount of embrittlement and strengthening, however, depended sensitively on implantation dose, implantation temperature, and tensile test temperature. The formation of helium bubbles, dislocation loops, and dislocation networks and the fracture modes were observed by transmission and scanning electron microscopy, respectively. Two ranges of embrittlement can be distinguished. They are attributed to different mechanisms: matrix strengthening is the dominant mechanism at low temperatures, and loss of grain boundary cohesion at high temperatures. It is concluded that in both temperature regimes the embrittlement is dominated by helium and not by the displacement defects introduced by its implantation.

1. Introduction

In a fusion reactor, the poisoning of the plasma by impurity atoms which are sputtered from the inner wall of the plasma containment, is reduced for low Z (light element) materials. Therefore, many test experiments have been carried out in order to use carbon-based materials and more recently also beryllium as candidates for plasma facing materials. Beryllium has an atomic number of only 4 and, being a metal of high mechanical stability and moderately good heat conductivity, may favourably be used also as structural material for components which are heavily bombarded by the particles escaping from the plasma. Radiation damage effects in these structural materials will be their life time limiting factor. Therefore many irradiation experiments have already been performed on light element materials including beryllium [1]. Those experiments are mostly carried out using fission reactor neutrons which are suitable to study the displacement damage effects. The fission reactor neutrons, however, having lower energies than the fusion neutrons, are unsuitable to properly evaluate a second radiation damage effect which originates from nuclear transmutation-produced helium via (n, α) processes. The production of helium via (n, α) nuclear reactions by the fusion neutrons increases strongly with decreasing Z of the target material. Therefore, helium implantation experiments emphasising the effects of transmutation-produced helium need to be adjoined to the fission reactor experiments which generally emphasise the displacement damage part of the radiation damage. From many studies on steels it is known how strongly mechanical properties, in particular at high temperatures, can be deteriorated by the presence of helium [2,3]. In the present work the effect of helium on strength and ductility of beryllium was investigated in tensile tests after helium implantation. The microstructure of the tensile-tested specimens was

* Corresponding author. Tel.: +49-2461-52794.
E-mail address: w.kesternich@fz-juelich.de (W. Kesternich).

0022-3115/03/$ - see front matter
PII: S0022-3115(02)01637-9

studied by transmission electron microscopy (TEM) and scanning electron microscopy (SEM).

2. Experimental

The specimen material was high purity (99.87%) beryllium. It had been delivered by Brush–Wellman as 0.2 mm thick foil, prepared from hot pressed powder by cross-rolling and subsequent annealing at 750 °C. According to the manufacturer the main impurities in wppm are 220 C, 200 BeO, 130 Fe, 60 Si, 45 Ni, and 45 Al. The average grain size, as determined by present SEM measurements, is about 50–70 μm. 3 mm wide specimen strips were cut from the foil material by spark erosion. The specimens were implanted by α particles from a 28 MeV cyclotron. The energy of the α particles was modulated by an aluminium degrader wheel in front of the specimen in such a way that the resulting helium deposition was homogeneous within the 0.2 mm specimen thickness. Homogeneous implantation density over the length and width of the specimen area was achieved by two-dimensional beam wobbling. The vacuum of the accelerator beam line was separated from the gas-filled specimen chamber by a 25 μm thick aluminium window. The specimens were irradiated in 400–600 mbar atmosphere of helium gas. The helium gas served for removal of the radiation-induced heat and for equilibrating the temperature between specimen and the heat sink to which the specimen was clamped on either end. The heat sink consisted of a nickel block containing a resistance heater. It was connected to a water cooling system in such a way that constant temperatures could be produced at the specimens in a range from below 80 to above 600 °C during the course of the irradiations. Two thermocouples were press-contacted to the specimen from below so that they were not exposed to the direct α particle beam. One thermocouple was positioned at the centre of the specimen and served to control the specimen temperature. The other was positioned 4 mm from the centre, near the end of the irradiated specimen area, for monitoring the temperature gradient along the specimen, resulting from the flux of radiation-induced heat towards the specimen clamps. The maximum temperature difference between the two thermocouple positions was measured at an irradiation temperature of 600 °C where it reached about 20 °C and where also the uncertainty of temperature measurement was highest: about 10 °C. Thus at nominally 600 °C, the irradiation temperature was (600 ± 10) °C at the specimen centre and (580 ± 10) °C at the ends of the irradiated area. Implantations were carried out at various temperatures between 100 and 600 °C to nominally equal helium contents of 220 appm and at 600 °C to a series of different concentrations. The α particle current density at the specimens was about 10 $\mu A/cm^2$ corresponding to an implantation rate of 1.5×10^{-5} appm/s. One of the specimens was annealed at 900 °C in vacuum in the 10^{-9} bar range after irradiation at 100 °C.

Tensile tests were performed on helium-implanted and unimplanted control specimens using a gauge length of 6 mm, which was positioned inside the irradiated area of 10 mm length. Fracture always took place at least 1.5 mm away from the specimen grips. The tensile test assembly was located inside a quartz tube which could be evacuated by turbomolecular pumping. The quartz tube was surrounded by a resistance heated oven which allowed tensile testing between room temperature and 700 °C. All tests were carried out in vacuum in the 10^{-9} bar range, with exception of some of the room temperature tests performed in air. The strain rates were always about 2.4×10^{-4} s^{-1}.

TEM specimens were prepared from the tensile-tested specimens by electropolishing, and the microstructure was investigated by 300 keV TEM. SEM was carried out in a microscope equipped with a field emission gun. The field emission source enables high resolution imaging in light element materials to be performed by using low accelerating voltages. Depending on the respective magnifications, voltages from 10 keV down to 1 keV have been applied in the present investigation.

3. Results

Two typical engineering stress–strain curves after 220 appm helium implantation are shown in Fig. 1. In both cases the implantation temperatures were equal to the tensile testing temperatures. Fracture was brittle with no indication of necking before rupture at 100 °C, and this was revealed to be typical for all tests at 100 °C and lower. At 300 °C ductile fracture is revealed. A

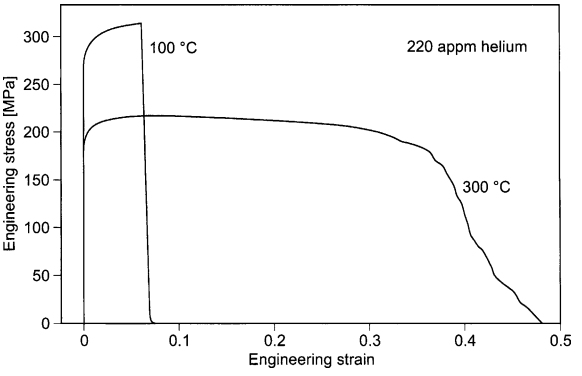

Fig. 1. Engineering stress–strain curves from tensile tests performed at 100 and 300 °C after helium implantation. Helium concentration was 220 appm. Implantation temperatures were equal to the tensile testing temperatures.

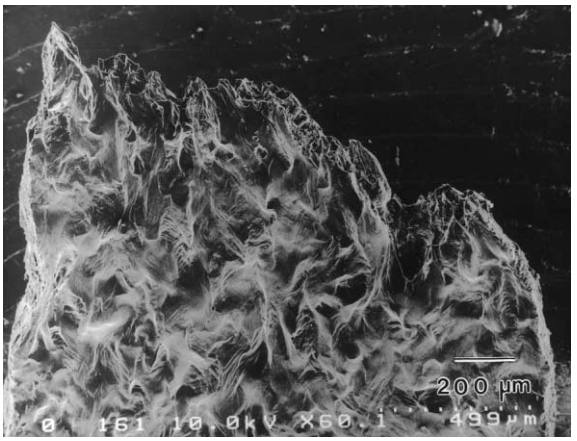

Fig. 2. Scanning electron micrograph of an unimplanted beryllium specimen tensile-tested at 200 °C.

range of uniform deformation is followed by a decrease in stress with a step-wise appearance in the stress–strain curves. The steps originate from a sequence of consecutive partial ruptures and further necking of the remaining specimen cross-section, as was indicated from fracture surfaces observed by SEM.

A scanning electron microscope image of an unirradiated specimen, tensile-fractured at 200 °C, is shown in Fig. 2. Non-uniform reduction of the specimen cross-section is clearly apparent, varying from one grain to another. The extent of necking varies along the fracture surface. The originally smooth outer specimen surface was transformed into a wavy surface, with wave lengths in correspondence with the grain sizes. The wave amplitude on surfaces of different specimens was higher for specimens with higher ductility. Yielding is obviously strongly dependent on the crystal orientations of the grains, and this is inferred to give rise to the step-wise occurrence of fracture, as revealed in stress–strain curves like the one for 300 °C in Fig. 1. Such step-wise fracture was commonly observed in stress–strain curves of specimens fractured in a ductile manner.

Six specimens were implanted at 600 °C with varying helium content between 30 and 800 appm. After implantation the specimens were tensile-tested at 600 °C. The results, together with the results from an unimplanted control specimen are shown in Fig. 3. Strain to fracture ε_f, 0.2% yield stress $\sigma_{0.2}$, and ultimate tensile stress σ_{UTS} are shown as a function of helium concentration. The three data points from the specimen containing 583 appm helium reveal a deviating behaviour far beyond the typical scattering of the data. The reason was not found, and the data points at 583 appm helium are disregarded in this work. Fig. 3 shows that the ductility decreased continuously with growing helium content. At 800 appm helium content it reaches about

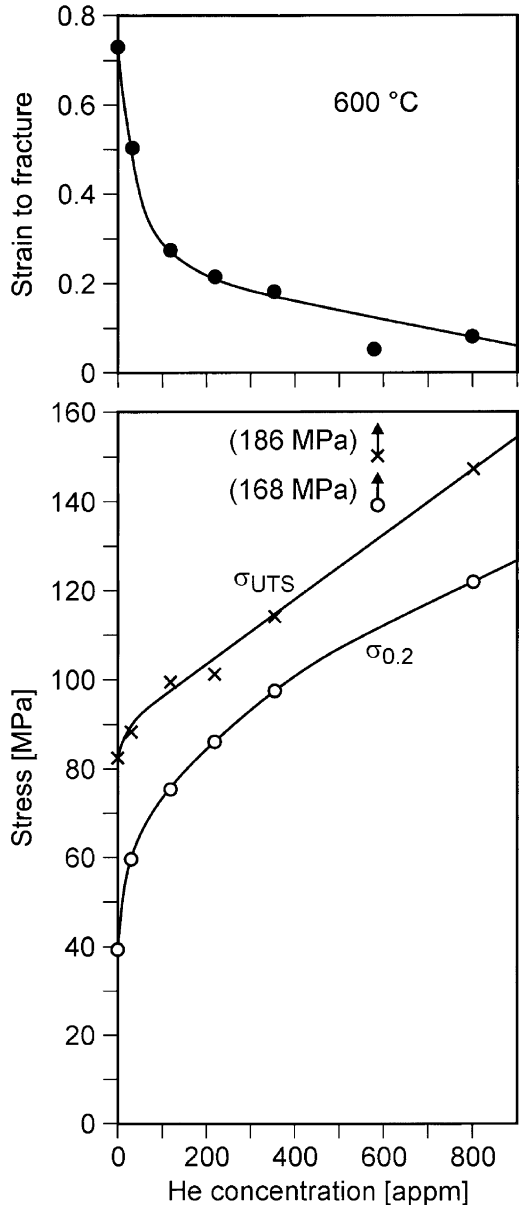

Fig. 3. Strain to fracture ε_f, 0.2% yield stress $\sigma_{0.2}$, and ultimate tensile stress σ_{UTS} as function of helium concentration for helium implantation and tensile testing at 600 °C.

10% of its pre-irradiation value. Simultaneously, yield strength and ultimate tensile strength grow by 200% and 80%, respectively. The line in Fig. 3 representing the yield strength as a function of helium concentration c_{He} is a fit to the dose relationship $\Delta\sigma_{0.2} = a\ (c_{He})^n$ where $\Delta\sigma_{0.2}$ is the yield stress with helium minus the yield stress without helium. The fit yields the values $a = 4.64$ MPa and $n = 0.43$. The lines in Fig. 3 representing the development of ultimate tensile strength and ductility are

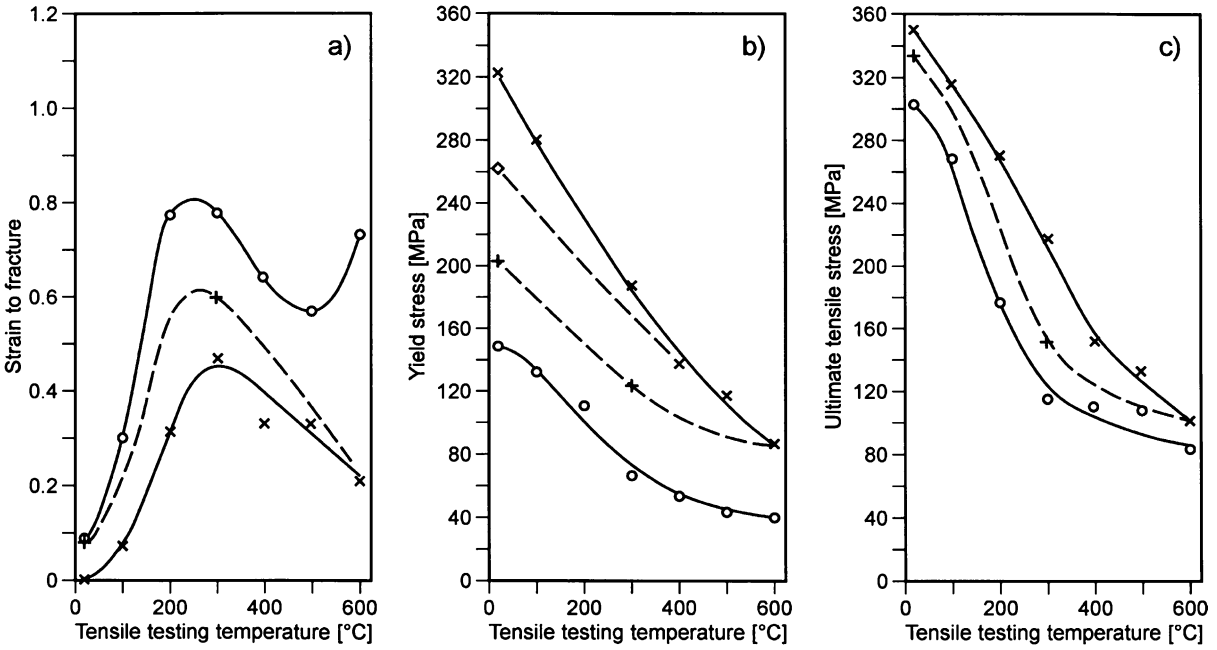

Fig. 4. Strain to fracture, yield stress, and ultimate tensile stress as a function of tensile testing temperature. ○ unimplanted; × implanted at the same temperatures as the tensile testing temperatures with exception of the data at room temperature where the implantation temperature was 100 °C; + implanted at 600 °C; ◇ implanted at 400 °C. Implantation doses are always 220 appm helium. Solid lines indicate the course of the data for unimplanted specimens and for those where the testing temperatures were equal to the implantation temperatures. Dashed lines are used to join data points of equal implantation temperatures.

just smooth curves which line up the experimental data and which may serve as an eye guide.

For 220 appm helium content, temperature dependences have been determined and are shown in Figs. 4 and 5. In Fig. 4 the implantation and tensile testing temperatures are identical, with the exception of the tensile test at room temperature. Since implantation at room temperature cannot be reached in the present irradiation chamber (the minimum is about 80 °C), this specimen was implanted at 100 °C. For comparison, corresponding tensile testing data on unimplanted specimens were experimentally determined and are included in Fig. 4. The ductility of unimplanted beryllium as a function of temperature shows a maximum at about 250 °C and after a local minimum at about 500 °C starts rising again. After 220 appm He implantation the ductility is reduced within the whole covered temperature range. The maximum in ductility is shifted slightly to higher temperatures, and the local minimum at 500 °C has disappeared. Both, yield strength and ultimate tensile strength were monotonously decreasing with increasing test temperature in the implanted specimens as in the unimplanted control specimens. For all temperatures yield strength and ultimate tensile strength increased as a result of helium implantation. The largest increases in yield strength were observed at room temperature and in ultimate tensile strength at an intermediate temperature of about 250 °C, which is close to the ductility maximum.

The mechanical property data measured as function of implantation temperature are presented in Fig. 5. All specimens were implanted to 220 appm helium content, and the tensile testing temperature was always room temperature. The fracture strain is only 0.008, at 100 °C. Beyond 100 °C, the ductility is rising rapidly with implantation temperature towards the value of the unimplanted specimen which is almost reached at 600 °C. The effect of helium on strength, particularly on the ultimate tensile strength, is less pronounced. At 100 °C, the difference between yield strength and ultimate tensile strength is only 7%, i.e. the specimen failed nearly in the elastic region. Reciprocally to the increasing ductilities, yield strength and ultimate tensile strength decrease with increasing temperature. Like the ductility values also both strength values tend towards their values for unimplanted beryllium.

The data points at 300 °C, from another measurement after implantation at 600 °C are added in each of the three plots in Fig. 4. The influence of helium on tensile strength and ductility was reduced as compared to the 300 °C implantation temperature. Another set of data points, transferred from Fig. 5 for room temperature tensile testing after 600 °C implantation, is added to Fig. 4. The data points for 600 °C implantation and

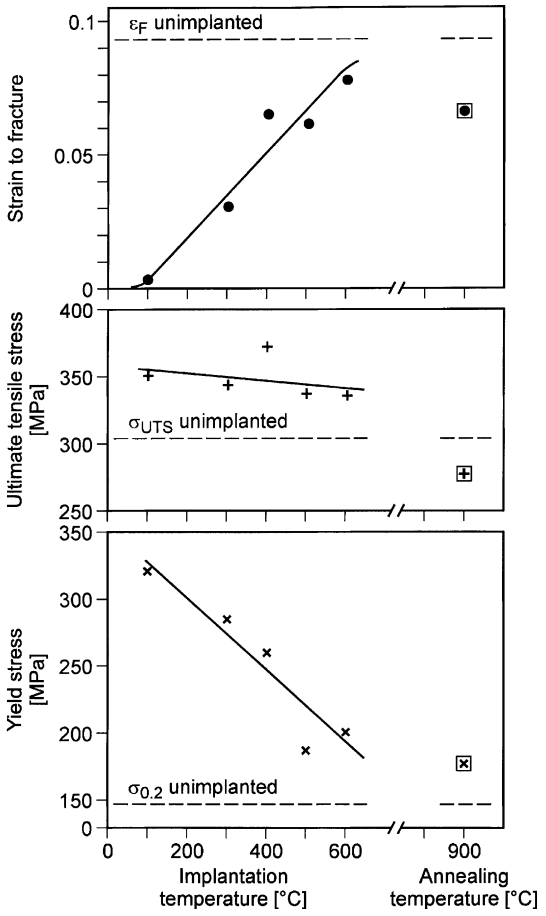

Fig. 5. Strain to fracture, yield stress, and ultimate tensile stress from tensile tests performed at room temperature after 220 appm helium implantation. Left side: data points as function of implantation temperature; right side: data from annealing at 900 °C for 2 h after He implantation at 100 °C. Dashed lines indicate the respective data of unimplanted beryllium.

testing at 20, 300 and 600 °C are joined by dashed lines. Further, another data point for 20 °C testing after 400 °C implantation and another dashed line are added for the respective 400 °C implantation data to the plot of the yield strength. These dashed lines indicate a general trend: compared to those experiments, where implantation and testing temperatures were equal, the influence of helium implantation is reduced when the implantation temperature is higher than the testing temperature, and this reduction is the stronger the higher this temperature difference is.

On the right side of Fig. 5, results of an annealing experiment are shown. Annealing was carried out at 900 °C for 2 h after He implantation at 100 °C to 220 appm and was followed by room temperature testing. The data at 900 °C thus should be compared to the data at 100 °C, i.e. for testing right after the implantation without additional annealing. The effect of helium on the room temperature mechanical properties is reduced by the high temperature anneal (data points at 900 °C, in comparison to 100 °C) in a similar way as by high temperature implantation (data points for 300–600 °C, in comparison to 100 °C). The effect on ultimate tensile strength is even inverted after the 900 °C anneal with respect to the helium-free specimen (dashed lines).

The microstructure of tensile-tested specimens was investigated by TEM and SEM. Fig. 6 shows a transmission electron micrograph taken after implantation of 220 appm helium at 100 °C and tensile testing at 100 °C. The visible microstructure in the matrix consists of dislocation networks and small dislocation loops. At higher temperatures helium bubbles are visible, i.e. at implantation temperatures of 400 °C and higher. With respect to this temperature, however, the resolution limit of TEM for helium bubbles of about 1–2 nm should be kept in mind. The micrograph in Fig. 7, containing the matrix and one grain boundary, was taken after 600 °C implantation of 800 appm helium and testing at 600 °C. Bubbles in the matrix have an average diameter of 30 nm. A high density of helium bubbles is revealed at the grain boundary, with an average bubble thickness of 10 nm. In general all bubbles in the matrix and at grain boundaries were faceted. As in Fig. 7, many grain boundaries were surrounded by bubble-denuded zones. At grain boundaries the bubbles were flattened perpendicular to the grain boundaries. This, together with the increased helium content at grain boundaries owing to the denuded zones leads to a significant perforation of grain boundary area by the respective bubble cross-sections and thus to losses in cohesion of the grain boundaries. The bubble size and density as well as the

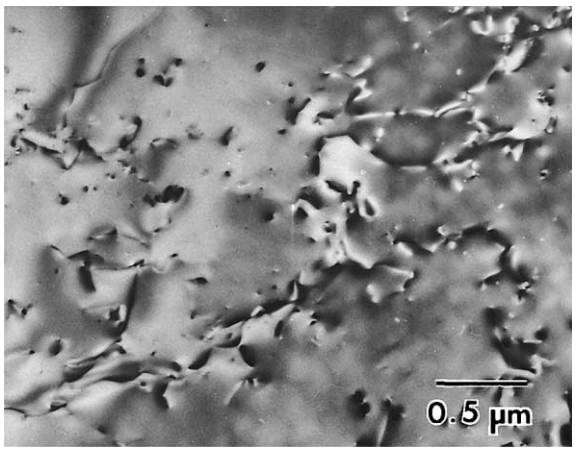

Fig. 6. Transmission electron micrograph of dislocation networks and dislocation loops produced by 220 appm helium implantation, accompanied by 0.02 dpa displacement damage, at 100 °C and tensile testing at 100 °C.

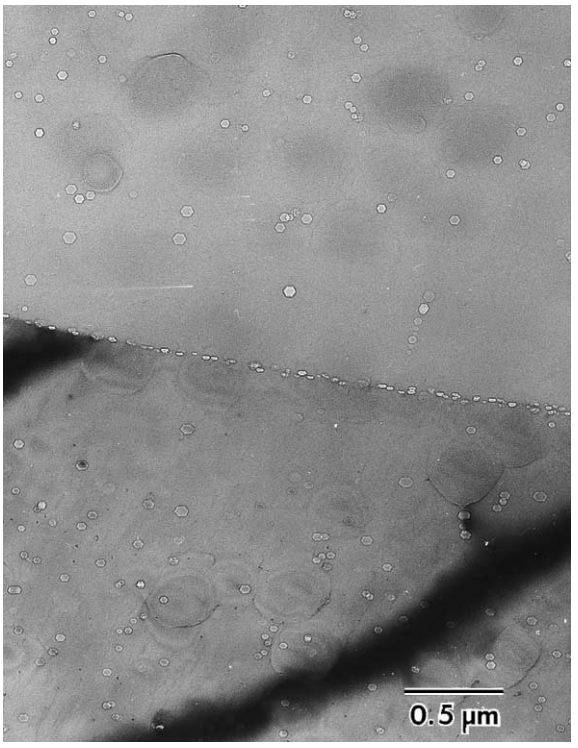

Fig. 7. Helium bubbles in the matrix and at a grain boundary after 800 appm helium implantation at 600 °C and tensile testing at 600 °C.

aspect ratio between bubble diameter and thickness, which together cause the loss in grain boundary cohesion, vary strongly from one boundary to another.

Fig. 8. Scanning electron micrograph of the outer surface of a specimen implanted with 600 appm helium at 600 °C and tensile-tested at 600 °C. The stress direction was close to vertical with respect to the figure.

Fig. 8 shows a scanning electron micrograph of the outer surface of a specimen implanted with 600 appm helium at 600 °C and tensile-tested at 600 °C. The vertical edge of the micrograph is parallel to the stress direction. Several cracks along grain boundaries can be observed as well as sequences of transgranular microcracks which are particularly clearly recognisable in the two grains at the right and the lower centre. The transgranular cracks were also observed after low temperature (20–200 °C) tests in unimplanted beryllium and in room temperature-tested specimens after low temperature (100–300 °C) implantation, the intergranular cracks only at 600 °C implantation and testing temperature and helium content higher than 50 appm. Within

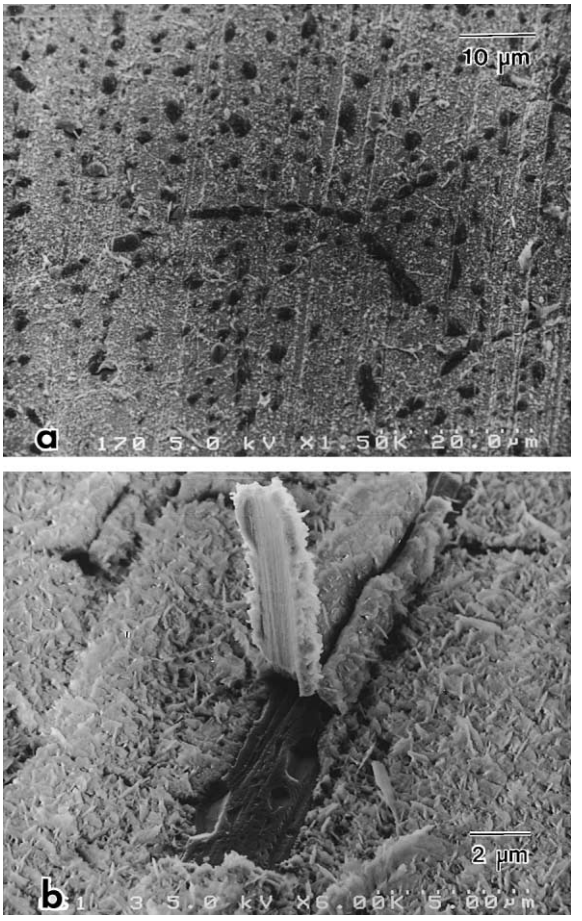

Fig. 9. Helium bubbles revealed at positions where the beryllium oxide layer has been split off, after (a) 600 and (b) 800 appm helium implantation at 600 °C and tensile testing at 600 °C. Where the surface layer is split off, 'surface' bubbles, as typically formed in the interfaces between BeO surface layer and beryllium metal, become visible. In (a) the location of grain boundaries becomes apparent by the high density of partly coalescing bubbles, in (b) a large flake of BeO is shown which had covered an assembly of bubbles of widely differing sizes.

the grains in Fig. 8 cavities of typically 2 μm diameter occur which are due to helium bubbles close to the surfaces. The reason for the occurrence of these bubbles is coverage of all specimen surfaces by thin BeO layers which obviously prevented helium from escaping out of the beryllium surfaces. As a result large helium bubbles were formed at elevated temperatures. They were observed to be located at the interfaces between the beryllium matrix and the BeO layer and were found to extend mainly into the beryllium metal and not into the beryllium oxide. The latter indicates that the surface tension is lower in Be than in BeO. Like bulk and grain boundary bubbles also all 'surface' bubbles were faceted.

Fig. 9 shows such 'surface' bubbles at specimen positions where the oxide layers have been split off. The specimens of Fig. 9(a) and (b) had received 600 and 800 appm helium implantation, respectively, at 600 °C and had been tensile-tested at 600 °C. The locations in Fig. 9(a) where the bubbles line up in particularly high densities, with bubbles partly touching and coalescing with each other, reveal the positions of the grain boundaries. Thus the high bubble density as observed in Be–BeO interfaces and in grain boundaries (see Fig. 7) was found to be further increased where those two types of interfaces intersect. In Fig. 9(b) part of a larger piece of split-off layer of BeO, which had covered several bubbles, is still attached to the specimen. The beryllium oxide layers have thicknesses of about 0.1–0.5 μm. Surface bubble sizes varied from 0.01 to 1 μm. Like in Fig. 9(a) and (b), the BeO layers have often been split off in large flakes (up to several μm), caused by the helium pressure in the bubbles and by the differential strain of Be and BeO. The high density of helium bubbles at the interfaces between beryllium metal and the relatively thin surface oxide layers indicates that helium permeation in BeO is lower than in Be. This 'sealing' of the metal surface by an oxide layer will strongly influence He diffusion measurements by the gas desorption method.

Simultaneous developments of transgranular and intergranular microcracks, such as revealed in Fig. 8, were the origin of alternating cleavage and intergranular fracture sections observed in the respective fracture surfaces. Part of such a fracture surface after the 900 °C annealing is shown in Fig. 10. About 60% of the fracture surface were intergranular and 40% of cleavage type after this pre-treatment. Many of the grain boundary facets of the intergranular fracture surfaces revealed dense coverage by helium bubbles which had grown under the influence of stress-induced coarsening. One example of four grain boundaries and one example of two grain boundaries and their intersections are shown in Fig. 11(a) and (b), respectively. Fig. 11(a) is a high magnification detail of Fig. 10. In general the bubbles on intergranular fracture surfaces were of widely varying sizes starting from the resolution limit for bubbles of about 20 nm (in Be for the field emission type SEM when operated at 1 keV accelerating voltage) and ranging up to several μm. Some grain boundaries, like the lower right one in Fig. 11(a), are almost free of bubbles. In Fig. 11(b) asymmetrical, but isomorphous faceting of bubbles at the grain boundary intersection is clearly apparent. The helium bubbles on cleavage sur-

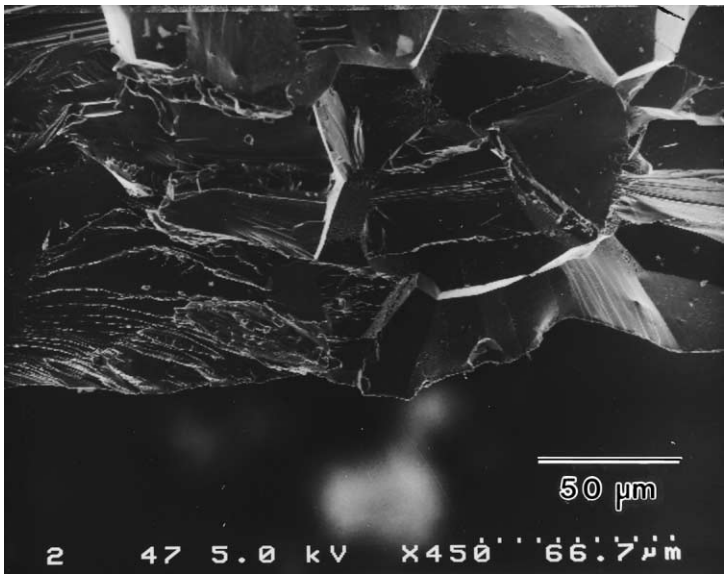

Fig. 10. Part of a fracture surface from a room temperature tensile test after 220 appm helium implantation at 100 °C and annealing at 900 °C. Cleavage fracture sections, often recognisable by sequences of cleavage steps, alternate with intergranular fracture sections, partly recognisable by their polyhedral appearance.

faces are generally below the SEM resolution limit, while bubbles on intergranular sections can be observed at implantation temperatures as low as 300 °C.

Cleavage is the predominant fracture mode for low temperature tensile testing. In two cases of low temperature testing, however, fracture surfaces revealed more than 50% intergranular surface area, i.e. for the specimens implanted at 100 °C and tested at room temperature with and without the 900 °C anneal. Ductile fracture appears as extended chisels or pointed tips such as in Fig. 2. Fracture surfaces were more than 50% ductile in unimplanted specimens from 200 to 600 °C and in specimens implanted and tensile-tested between 300 and 500 °C. Table 1 shows the fractions of different fracture modes for the investigated implantation and tensile testing conditions.

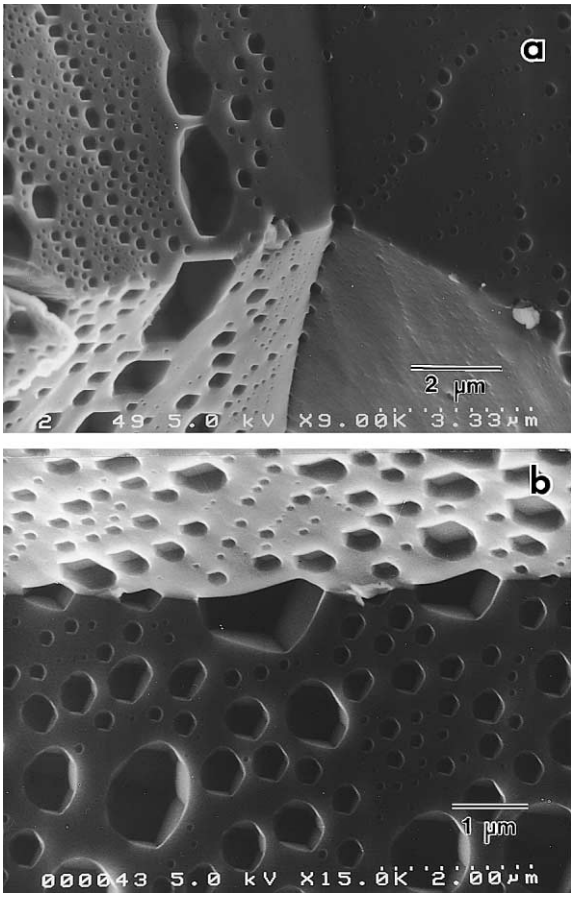

Fig. 11. Examples of intergranular fracture sections from the same specimen as in Fig. 10. (a) Four intersecting grain boundaries. The grain boundary facets are covered by faceted bubbles of widely varying size down to the resolution limit in SEM. (b) Bubbles at grain boundary intersections are faceted asymmetrically, but are isomorphous with each other.

4. Discussion

Beryllium has many desirable properties with respect to the use as structural material. In particular the *E*-modulus–density ratio of beryllium is the highest of any metal. The fracture behaviour, however, gives rise to limitations in its applicability. There is a transition from brittle to ductile fracture above room temperature, and so far it was not possible to shift this transition temperature to below room temperature by any metallurgical means. In casted beryllium the strain to fracture ε_f is practically zero, in powder metallurgically prepared beryllium, however, ε_f may have values up to 0.1. At elevated temperatures (200–300 °C), the ductility is significantly higher, and in high purity beryllium ductility beyond 300 °C can be raised by annealing treatments at 700–800 °C. Such type of beryllium, powder metallurgically manufactured and heat treated for high ductility, is used in this study.

In the present experiments the influence of helium content on tensile strength and ductility has been investigated for various combinations of implantation temperature, tensile testing temperature, and annealing temperature for nearly the same helium content of close to 220 appm (see Figs. 4 and 5). The resulting values of strain to fracture and 0.2% yield stress are schematically summarised in a temperature diagram in Fig. 12. The upper left triangle of the temperature diagram, i.e. the range with tensile testing temperature larger than implantation temperature has no practical importance and therefore has not been included in this investigation. At the left side in Fig. 12 the values for umimplanted control specimens are listed.

For the case implantation temperature and testing temperature both equal to 600 °C, the influence of helium has been studied up to concentrations of 800 appm (Fig. 3) It should be noted that 800 appm helium produced by (n, α) reactions will be typically reached within half a year of fusion reactor operation.

4.1. Strengthening an effect of helium implantation or displacement damage?

For all testing and implantation temperatures applied in the present study, yield strength is increased and ductility is decreased as compared to the unimplanted specimens. The question arises whether the effects of implantation on the tensile properties result from helium or from lattice defects introduced during the implantation. It is known that in other metals helium bubble formation in grain boundaries with resulting weakening of the grain boundaries dominates the mechanical properties at high temperatures (i.e. at $>0.5\ T_m$, where T_m is the melting temperature in K). Grain boundary helium bubbles lead to the well-known effects of high temperature helium embrittlement. In the present

Table 1
Percentage of fracture modes in the fracture surfaces of beryllium specimens as observed by SEM after the different implantation, annealing and tensile testing treatments

Implantation, annealing and tensile testing condition		Percentage of fracture mode		
		Ductile	Brittle[a]	Intergranular
Unirradiated	Tensile test at 20 °C	0	95 c	5
	Tensile test at 100 °C	5	90 c	5
	Tensile test at 200 °C	100	0	0
	Tensile test at 300 °C	95	5	0
	Tensile test at 400 °C	100	0	0
	Tensile test at 500 °C	100	0	0
	Tensile test at 600 °C	100	0	0
50 appm He implantation at 600 °C	Tensile test at 600 °C	90	10 t	0
100 appm He implantation at 600 °C		50	35 t	15
200 appm He implantation at 600 °C		40	35 t	25
350 appm He implantation at 600 °C		45	25 t	30
580 appm He implantation at 600 °C		20	40 t	40
800 appm He implantation at 600 °C		20	40 t	40
220 appm He implantation at 100 °C	Tensile test at 100 °C	0	90 c	10
220 appm He implantation at 200 °C	Tensile test at 200 °C	5	90 c	5
220 appm He implantation at 300 °C	Tensile test at 300 °C	98	2 c	0
220 appm He implantation at 400 °C	Tensile test at 400 °C	100	0	0
220 appm He implantation at 500 °C	Tensile test at 500 °C	80	20 t	0
220 appm He implantation at 600 °C	Tensile test at 600 °C	40	35 t	25
220 appm He implantation at 100 °C	Tensile test at 20 °C	0	45 c	55
220 appm He implantation at 300 °C		0	80 c	20
220 appm He implantation at 400 °C		0	70 c	30
220 appm He implantation at 500 °C		0	80 c	20
220 appm He implantation at 600 °C		0	95 c	5
220 appm He implantation at 100 °C, annealing at 900 °C	Tensile test at 20 °C	0	40 c	60
220 appm He implantation at 600 °C	Tensile test at 20 °C	0	95 c	5
	Tensile test at 300 °C	100	0	0
	Tensile test at 600 °C	40	35 t	25

[a] c: cleavage, t: transgranular non-cleavage.

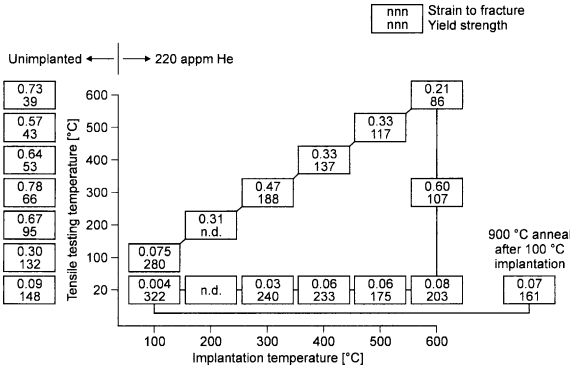

Fig. 12. Schematical temperature diagram of strain to fracture and yield strength.

experiments on beryllium high densities of helium bubbles were observed in grain boundaries (see Fig. 7) at 400 °C (0.43 T_m) and higher which suggests that the impact of helium is dominant at high temperatures also in beryllium. At low temperatures, however, the importance of helium for the mechanical strength and ductility is in question. E.g. for room temperature helium implantations in high alloy steels, displacement damage and not helium has been found to be responsible for the radiation-induced strengthening, at least up to 5000 appm helium content [4].

Calculations using the TRIM94 simulation computer program taking into account the presently applied energy degrading of the α particles for homogeneous depth distribution of helium inside the specimens, resulted in an inhomogeneous distribution of displacement damage with He/dpa ratios (i.e. helium atom per atom/atomic displacement per atom) between 0.10 and 0.17 at the entrance and exit surface of the beryllium specimens, respectively. Thus for the experiments on temperature

dependences which were all performed with 220 appm He, the displacement damage was very low, varying from 0.023 to 0.013 dpa at entrance and exit surface of the specimens, respectively.

Helium is insoluble in metals and is considered here as either trapped in single vacancies or precipitated into helium bubbles. For the case that helium atoms are present in single helium-vacancy complexes, the helium-induced strengthening $\Delta\sigma_{0.2}$ can be estimated by applying the standard equation for solid solution strengthening [5]

$$\Delta\sigma_{0.2} = (M/700)\mu c_{\mathrm{He}}^{1/2}\delta^{3/2}, \quad (1)$$

where M relates the shear stress in a slip plane to the tensile stress in a polycrystal, μ is the shear modulus, c_{He} is the helium concentration, and δ is a parameter characterising the modulus and size interaction between solute atoms and dislocations. With $M = 3$, $\delta = 1$, $\mu = 1.5 \times 10^{10}$ Pa, and $c_{\mathrm{He}} = 2.2 \times 10^{-4}$, Eq. (1) yields $\Delta\sigma_{0.2} = 1$ MPa. This is two orders of magnitude less than the experimental values. Hence the hardening cannot be attributed to solution hardening by single helium atoms.

For the case that helium is present in small bubbles, the Orowan mechanism for dislocation pinning at precipitates may be applied, and the strength increase $\Delta\sigma_{0.2}$ can be estimated from [6,7]

$$\Delta\sigma_{0.2} = (M\mu b/\lambda)\cos(\theta/2), \quad (2)$$

where b is the Burgers vector of the moving dislocations, λ is the distance between obstacles in the glide plane, and θ is the critical bow-out angle of the dislocation at the obstacle, thus defining the strength of the obstacle. Analogous to helium cluster densities in steel [8] $\lambda = 10$ has been estimated in beryllium taking into account the present homologous temperature ($0.24T_{\mathrm{m}}$) at 100 °C and helium production rate (1.5×10^{-2} appm/s). With $M = 3$, $\mu = 1.5 \times 10^{10}$ Pa, and $b = 0.2$ nm, Eq. (2) yields $\Delta\sigma_{0.2} = 900$ MPa for $\cos(\theta/2) = 1$ ($\theta = 0$), which is the ideal case of Orowan pinning on strong obstacles, and $\Delta\sigma_{0.2} = 175$ MPa for $\cos(\theta/2) = 0.2$, a value proposed for small helium bubbles, representing weak obstacles in steels [7]. These values are not sensitively dependent on cluster size, and apply well for clusters or bubbles containing 3–100 helium atoms, while for large bubbles a value $\cos(\theta/2) = 1$ is expected. The latter $\Delta\sigma_{0.2}$ value agrees well with our experimental values of 174 and 148 MPa after 100 °C implantation and testing at 20 and 100 °C, respectively. A direct determination of λ is possible at high temperatures. At 600 °C and 800 appm, λ can be roughly estimated from TEM micrographs (see Fig. 7) to be 150 nm. Using this number in Eq. (2) and the experimental value of $\Delta\sigma_{0.2} = 80$ MPa, results in $\cos(\theta/2) = 1$, suggesting that the large bubbles, observed at high temperatures, act as strong obstacles.

Nevertheless, also pinning on interstitial atom clusters and small dislocation loops may result in strengthening effects similar as calculated for helium bubbles from Eq. (2). The microstructure (see Fig. 6) shows such irradiation-induced dislocation loops to be present after the low temperature helium implantations. Therefore a comparison with other irradiation sources of differing helium/dpa ratio is used here in order to decide whether helium or lattice defects are dominating the observed strengthening.

At 200 °C irradiation temperature a comparison with recent neutron irradiations by Moons et al. [9] is possible. With ≈1 dpa and 600 appm He they measure an increase in yield stress $\Delta\sigma_{0.2}$ by 190 MPa. Interpolation of the present data to the same temperature (implantation at 200 °C, cf. Fig. 4) with 0.02 dpa and 220 appm helium yields a value of $\Delta\sigma_{0.2} = 154$ MPa. Both experiments reveal a strength increase by the same order of magnitude and for the same order of helium content, while in our experiment the displacement damage was lower by two orders of magnitude than in the neutron irradiation experiment.

Another comparison with neutron irradiation results (not only in the same range of the present helium concentrations, but also in the same range of the present displacement damage values) is possible with irradiation temperature and tensile testing temperature both at 300 °C [10]. Present results for 220 appm helium and about 0.02 dpa at 300 °C revealed a yield stress increase by $\Delta\sigma_{0.2} = 121$ MPa. Snead [10] measured a stress increase after neutron irradiation of $\Delta\sigma_{0.2} = 10$ MPa at 0.04 dpa, corresponding to 10 appm He, and a value of $\Delta\sigma_{0.2} = 125$ MPa at 0.74 dpa, corresponding to 190 appm He. The former neutron result is obtained for a dpa value, the latter for an appm He value similar to the respective present ones. Comparing the respective yield stresses in the present results and in both neutron irradiation results, indicates that helium is responsible for the radiation-induced strengthening in beryllium.

It needs to be considered, however, that helium clusters may increase the nucleation rate of dislocation loops and in general stabilise displacement defects. At least in steels this is concluded from helium implantation experiments. Thus the observed strengthening could arise from defects trapped by helium bubbles rather than directly from the helium bubbles. However, the comparison of the helium implantation and neutron irradiation experiments show that in the former the combined effect of number density and pinning strength of the defects needs to be enhanced by a factor of 30. This appears unlikely.

Therefore it is concluded that the helium and not the displacement damage is mainly responsible for the irradiation strengthening after low temperature helium implantation. This conclusion has at first been drawn for the present 220 appm helium concentration. The effect

of helium, however, is expected to be even more dominant at higher implantation doses, since the displacement damage effects tend to saturate at higher doses (usually below 1 dpa, due to linking of dislocation loops into networks). The dominance of helium applies to the present He/dpa ratio of 0.015, but according to the above comparisons may possibly extend also to the lower He/dpa ratios of 0.00025 in the considered fission neutron irradiations.

4.2. Effect of helium bubble growth on strengthening

In all of the present experimental results helium has led to increases of yield strength and ultimate tensile strength with the exception of the 900 °C annealing experiment. Generally the effect of helium on yield strength has been stronger than on the ultimate tensile strength with again the exception of the 900 °C annealing experiment. The increases in yield strength are accompanied by decreases in ductility. The relative amount of ductility loss at low temperatures is higher than at high temperatures. This behaviour suggests that in the whole temperature range with the exception of 900 °C, helium is mainly effective in the matrix and not in the grain boundaries, and that helium strengthens the matrix in combination with a corresponding loss in ductility by pinning of dislocations at helium clusters. If embrittlement, owing to weakening of the grain boundary cohesion, would be the dominant effect a simultaneous loss of strength and ductility and not an increase in strength should take place, in a similar way as it is observed for high temperature helium embrittlement in steels and nickel-base alloys. Possibly, up to 500 or 600 °C, helium clusters in the matrix are effective in impeding dislocation motion and thus reducing the extent of plastic deformation.

At a given tensile testing temperature the influence of helium was strongest when implanted at the temperature of testing, and the helium effects were the more reduced the more the implantation temperature surpassed the testing temperature. This is revealed in Fig. 5 for room temperature testing and is indicated by the dashed curves in Fig. 4 for elevated temperatures. This suggests that the reduction in bubble density caused by the smaller nucleation rate at higher implantation temperatures leads to less efficient dislocation pinning. This effect cannot be compensated by the resulting larger bubble sizes because the pinning is rather insensitive to the obstacle size (see Eq. (2)).

4.3. Helium embrittlement resulting from matrix strengthening and grain boundary weakening

The experiment with 900 °C annealing after 100 °C implantation, followed by testing at room temperature, is the only one where the yield strength was almost unchanged and the ultimate tensile strength was even reduced with respect to the corresponding room temperature test of unimplanted material. The possible reason could be grain growth. Since the beryllium specimens had been stress annealed at 750 °C before the present experiments, the 900 °C annealing after helium implantation could have changed the grain size and thus led to a reduction in strength. From grain size measurements by SEM it was found, however, that the grain size was not altered by the 900 °C anneal.

Therefore it is proposed that the strength reduction is caused by the observed changes in bubble population. The TEM and SEM investigations both show large numbers of helium bubbles at grain boundaries in the 500 and 600 °C implantation and 900 °C annealing experiments. At 900 °C the grain boundary bubbles have grown to much larger sizes than the matrix bubbles and cover large areas of many of the boundaries (see Fig. 11). The TEM results at 600 °C further show bubble-denuded zones adjacent to grain boundaries with a correspondingly enhanced helium density in the boundaries (see Fig. 7). The resulting reduction in grain boundary cohesion is generally the origin of high temperature helium embrittlement, as it is observed, for instance, in austenitic steels, and is inferred to be also operative here at temperatures higher than 500 or 600 °C. Eventually at 900 °C grain boundary-related helium embrittlement apparently dominates so much over matrix strengthening that the ultimate tensile strength has been reduced in comparison to the unimplanted specimens.

4.4. Ductility maximum and minimum

As revealed in Fig. 4, the data on the temperature dependence of strain to fracture in unimplanted beryllium show a maximum at about 250 °C and a minimum at about 500 °C. Such maxima and subsequent minima are typical of beryllium. The position of the maximum depends on grain size and is further slightly dependent on the impurity atom content. For the presently observed 50–70 μm grain diameter the maximum is typically located at 200–300 °C. The height of the maximum increases with grain size, but also sensitively depends on impurity content in a not yet understood way. At further increased temperatures in high purity, sintered beryllium a ductility minimum occurs, the origin of which cannot be explained. One of the effects of the present helium implantation was that the maximum together with the transition temperature from brittle to ductile fracture is shifted to slightly higher temperatures (see Fig. 4). With respect to this temperature shift helium appears to act in the same way as a typical impurity atom.

Another observation in Fig. 4(a) is that the ductility minimum at 500 °C has disappeared after helium im-

plantation. The temperature $0.5T_m$, which is regarded as the approximate onset of the classical range of helium embrittlement, is 504 °C in beryllium. The addition of grain boundary-related helium embrittlement to helium-induced matrix strengthening has apparently led to an additional loss in ductility at 600 °C and thus made the minimum to disappear.

5. Conclusion

Ductility losses of beryllium caused by helium implantation have been measured between 20 and 600 °C. As a conclusion from the present study, two embrittlement mechanisms operating in two different temperature regimes can be distinguished. The low temperature regime, up to 500 °C, is dominated by strengthening of the matrix accompanied by losses in ductility. From comparison with data of reactor irradiations, it is inferred that this strengthening is dominated by dislocation pinning at small helium clusters and not at the implantation-induced lattice defects. At high implantation or annealing temperatures, i.e. 600 °C and higher, helium embrittlement in the conventional sense is operative. It is caused by grain boundary weakening resulting from preferential helium bubble growth in grain boundaries.

The highest relative ductility loss was observed at 100 °C implantation and 20 °C tensile testing though the unimplanted beryllium was already brittle at room temperature. The highest absolute loss in ductility was observed for implantation and tensile testing at 600 °C. The latter is probably caused by the additive effect of both embrittling mechanisms, i.e. matrix hardening, and grain boundary weakening. At 900 °C the grain boundary-related embrittlement was dominant.

The strengthening and embrittling effects were strongest when implantation temperatures were equal to the test temperatures while they were increasingly reduced the more the implantation temperature surpassed the test temperature. This suggests that dislocation pinning at helium bubbles was most efficient when the bubble density was high, resulting in bubble sizes below the visibility limit of TEM. The pinning effect was reduced concurrent with the decreased bubble nucleation density at increasing implantation temperatures and also with the reduced bubble density as a result of annealing.

In the covered concentration range between 50 and 800 appm helium a tendency towards saturation with dose was observed, but full saturation was not reached at 800 appm helium. The presently observed large helium embrittlement effects suggest that helium, as created by nuclear reactions, may cause serious problems for the application of beryllium in components of future fusion reactors which are subject to mechanical loads.

Summarising the microstructural investigations, it was observed that:

1. At low tempertatures, helium implantation caused a transition from cleavage to intergranular fracture.
2. With 220 appm He, only at temperatures of 400 °C and higher, helium bubbles were visible by TEM. It is concluded, however, that already at an implantation temperature of 100 °C, small helium clusters were formed in the matrix.
3. In the high temperature regime, an increasing density of helium bubbles was observed either by increasing the implantation dose or decreasing the implantation temperature. Both led to an increasing replacement of ductile fracture by brittle transgranular and intergranular failure.
4. At 600 °C and higher temperatures, grain boundaries and intergranularly fractured surfaces were covered with dense arrays of facetted bubbles, with denuded zones surrounding the grain boundaries.

Acknowledgements

The indispensable assistance of W. Schmitz during implantation, tensile testing and scanning electron microscopy and the preparation of the thin specimens required for the electron microscopy by H. Klein is gratefully acknowledged.

References

[1] D.S. Gelles, G.A. Sernyaev, M. Dalle Donne, H. Kawamura, J. Nucl. Mater. 212–215 (1994) 29;
F. Scaffidi-Argentina (Ed.), Proceedings of the Fourth IEA International Workshop on Beryllium Technology for Fusion, FZKA Report 6462 (2000).
[2] H. Schroeder, W. Kesternich, H. Ullmaier, Nucl. Eng. Des./Fusion 2 (1985) 65.
[3] H. Schroeder, H. Ullmaier, J. Nucl. Mater. 179–181 (1991) 118.
[4] H. Ullmaier, E. Camus, J. Nucl. Mater. 251 (1997) 262;
H. Ullmaier, J. Chen, J. Nucl. Mater., in press.
[5] R.L. Fleischer, in: D.M. Peckner (Ed.), The Strengthening of Metals, Reinhold, New York, 1964, p. 93.
[6] U.F. Kocks, A.S. Argon, M.F. Ashby, Progr. Mater. Sci. 19 (1975) 1.
[7] G.E. Lucas, J. Nucl. Mater. 206 (1993) 287.
[8] H. Trinkaus, H. Ullmaier, J. Nucl. Mater. 296 (2001) 101;
H. Tinkaus, private communication.
[9] F. Moons, L. Sannen, A. Rahn, J. Van de Velde, J. Nucl. Mater. 233–237 (1996) 823.
[10] L.L. Snead, Oak Ridge National Laboratory, Fusion Materials Semiannual Report DOE/ER-0313/24 (1998) 215.